ELSEVIER

Comput. Methods Appl. Mech. Engrg. 191 (2002) 5877–5897

Computer methods in applied mechanics and engineering

www.elsevier.com/locate/cma

A posteriori discontinuous finite element error estimation for two-dimensional hyperbolic problems

Slimane Adjerid *, Thomas C. Massey [1]

Department of Mathematics and Interdisciplinary Center for Applied Mathematics, Virginia Polytechnic Institute and State University, Blacksburg, VA 24061-0123, USA

Received 27 June 2002

Abstract

We analyze the discontinuous finite element errors associated with p-degree solutions for two-dimensional first-order hyperbolic problems. We show that the error on each element can be split into a dominant and less dominant component and that the leading part is $O(h^{p+1})$ and is spanned by two $(p+1)$-degree Radau polynomials in the x and y directions, respectively. We show that the p-degree discontinuous finite element solution is superconvergent at Radau points obtained as a tensor product of the roots of $(p+1)$-degree Radau polynomial. For a linear model problem, the p-degree discontinuous Galerkin solution flux exhibits a strong $O(h^{2p+2})$ local superconvergence on average at the element outflow boundary. We further establish an $O(h^{2p+1})$ global superconvergence for the solution flux at the outflow boundary of the domain. These results are used to construct simple, efficient and asymptotically correct a posteriori finite element error estimates for multi-dimensional first-order hyperbolic problems in regions where solutions are smooth.

1. Introduction

The discontinuous Galerkin method (DGM) was first used for the neutron equation by Reed and Hill [20]. Since then, DGM methods have been used to solve hyperbolic [4–7,11–13,16], parabolic [14,15], and elliptic [2,3,23] partial differential equations. For a more complete list of citations on the DGM and its applications consult [10].

The DGM has been used successfully to solve systems of hyperbolic systems of conservation laws. The DGM method has several advantages over continuous methods, since it uses completely discontinuous polynomial bases it can sharply capture discontinuities which are common for hyperbolic problems and makes order variations and mesh refinement much easier in the presence of hanging nodes. The DGM has a simple communication pattern that makes it useful for parallel computations.

* Corresponding author.
E-mail address: adjerids@calvin.math.vt.edu (S. Adjerid).
[1] Present address: Naval Research Laboratory, Oceanography Division (7322), Stennis Space Center, MS 39528, USA.

0045-7825/02/$ - see front matter
PII: S0045-7825(02)00502-9

A posteriori error estimates have been an integral part of every adaptive method, thus for the DGM to be used in an adaptive setting one needs to develop a posteriori error estimates that will be used to guide the adaptive process by indicating regions where more or less resolution is needed, to assess the quality of the solution and to stop the adaptive process. A variety of a posteriori error estimates for DG methods have been developed by Bey and Oden [4], Süli [22] and Rivière and Wheeler [21] for linear problems. For nonlinear problems consult [8,9,19].

Adjerid et al. [1] proved that smooth DGM solutions of one-dimensional hyperbolic problems using p-degree polynomial approximations have an $O(h^{p+2})$ superconvergence rate at the roots of Radau polynomial of degree $p+1$. They used this result to construct asymptotically correct a posteriori error estimates. They further established a strong $O(h^{2p+1})$ superconvergence at the downwind end of every element. Krivodonova and Flaherty [18] proved a superconvergence result on average on the outflow edge of every element of unstructured triangular meshes and constructed a posteriori error estimates that converge to the true error under mesh refinement.

In this paper we extend the one-dimensional results of Adjerid et al. [1] to multi-dimensional hyperbolic problems on rectangular meshes. We show how to select the finite element space such that the leading term in the true local error is spanned by two $(p+1)$-degree Radau polynomials in the x and y directions, respectively. The p-degree discontinuous finite element solution exhibits an $O(h^{p+2})$ superconvergence at the Radau points obtained as a tensor product of the roots of Radau polynomial of degree $p+1$. For a linear model problem we show that, locally, the solution flux is $O(h^{2p+2})$ superconvergent on average on the outflow element boundary. We further show that the solution flux converges at an $O(h^{2p+1})$ rate on average at the outflow boundary of the domain. We use these superconvergence results to construct asymptotically correct a posteriori error estimates.

The paper is organized as follows, in Section 2 we present the error analysis and new superconvergence results. In Section 3 we construct several a posteriori error estimates for linear and nonlinear problems. We present computational results for several linear and nonlinear problems in Section 4. The computational results suggest that the theory of Section 2 extends to more general situations such as nonlinear conservation laws and solutions with discontinuities, except for the flux superconvergence which is under further investigation. We conclude and discuss our results in Section 5.

2. Error analysis

We begin our error analysis by considering the linear first-order model problem

$$\boldsymbol{\alpha}\cdot\nabla u = f(x,y), \qquad (x,y)\in\Omega=[0,1]\times[0,1], \tag{2.1a}$$

subject to the boundary conditions at the inflow boundaries

$$u(x,0)=g_0(x) \quad \text{and} \quad u(0,y)=g_1(y). \tag{2.1b}$$

Let $\partial\Omega=\partial\Omega_{\text{in}}\cup\partial\Omega_{\text{out}}$ denote the boundary of Ω and $\boldsymbol{\nu}$ be the outward unit normal to $\partial\Omega$. The inflow boundary is

$$\partial\Omega_{\text{in}}=\{(x,y)\in\partial\Omega|\boldsymbol{\alpha}\cdot\boldsymbol{\nu}<0\} \tag{2.2a}$$

and the outflow boundary is

$$\partial\Omega_{\text{out}}=\{(x,y)\in\partial\Omega|\boldsymbol{\alpha}\cdot\boldsymbol{\nu}>0\}. \tag{2.2b}$$

We assume that $\boldsymbol{\alpha}=[\alpha_1,\alpha_2]^{\mathrm{T}}$ is constant with $\alpha_i>0$, $i=1,2$. The functions $f(x,y)$, $g_0(x)$ and $g_1(y)$ are selected such that the exact solution $u(x,y)\in C^{\infty}(\Omega)$.

In order to obtain a weak discontinuous Galerkin formulation, we partition the domain Ω into $N = n \times n$ square elements and start the integration with elements whose inflow boundary is on the domain inflow boundaries. In order to perform an error analysis we consider the first element $\Delta = [0, h]^2$ where $h = 1/n$ and the space $\mathscr{V}_p$ of polynomial functions such that

$$\mathscr{P}_{p+1} \subset \mathscr{V}_p \cup \{x^{p+1}, y^{p+1}\}, \quad p \geqslant 0, \tag{2.3a}$$

where $\mathscr{P}_k$ is the space of polynomials of degree k

$$\mathscr{P}_k = \left\{ q | q = \sum_{m=0}^{k} \sum_{i=0}^{m} c_i^m x^i y^{m-i} \right\}. \tag{2.3b}$$

These spaces are suboptimal but they lead to a very simple a posteriori error estimator. For efficiency reasons we consider the smallest spaces that satisfy (2.3a) and (2.3b)

$$\mathscr{V}_p = \left\{ V | V = \sum_{k=0}^{p} \sum_{i=0}^{k} c_i^k x^i y^{k-i} + \sum_{i=1}^{p} c_i^{p+1} x^i y^{p+1-i} \right\}. \tag{2.4}$$

We note that tensor product elements satisfy (2.3a) and (2.3b).

The DGM [17] consists of determining $U(x, y) \in \mathscr{V}_p$ on Δ such that

$$\int_{\Gamma_{\text{in}}} \boldsymbol{\alpha} \cdot \boldsymbol{\nu} V (U^- - U) \, \mathrm{d}\sigma + \iint_{\Delta} \boldsymbol{\alpha} \cdot \nabla U V \, \mathrm{d}x \, \mathrm{d}y = \iint_{\Delta} f(x, y) V \, \mathrm{d}x \, \mathrm{d}y, \quad \forall V \in \mathscr{V}_p, \tag{2.5}$$

where $\Gamma = \Gamma_{\text{in}} \cup \Gamma_{\text{out}}$ is the boundary of Δ, with Γ_{in} and Γ_{out}, respectively, denoting the inflow and outflow boundaries of Δ as shown in Fig. 1. For the boundary data U^- on Γ_{in} we use either the exact boundary condition or its interpolant

$$U^-(x, y) = \begin{cases} \pi g_0 & \text{if } (x, y) \in \Gamma_1, \\ \pi g_1 & \text{if } (x, y) \in \Gamma_4, \end{cases} \tag{2.6}$$

where πw is the p-degree polynomial that interpolates w at the roots of $(p+1)$-degree right Radau polynomial

$$R_{p+1}(\xi) = L_{p+1}(\xi) - L_p(\xi), \quad -1 \leqslant \xi \leqslant 1 \tag{2.7}$$

with L_p being Legendre polynomial of degree p.

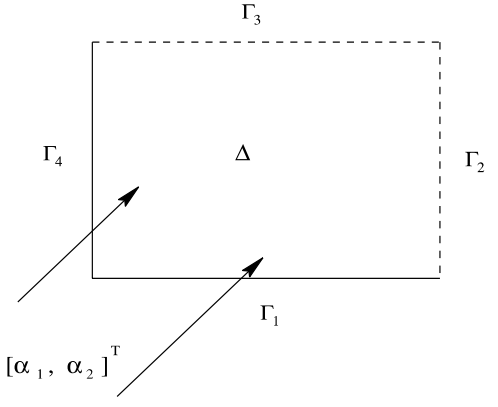

Fig. 1. An element Δ with inflow (solid) and outflow (dashed) boundaries.

Once we determine the solution on the first element Δ we proceed to the elements whose inflow boundaries are either on the inflow boundary of Ω or an outflow boundary of Δ and continue this process until the solution is determined in the whole domain. On an element whose inflow boundary is not on the boundary of Ω, U^- is defined as

$$U^-(x,y) = \lim_{s\to 0^+} U((x,y) + s\boldsymbol{v}), \quad (x,y) \in \Gamma_{\text{in}}. \tag{2.8}$$

We will show that the discontinuous Galerkin local finite element error can be split into an $O(h^{p+1})$ component which is a linear combination of two right Radau polynomials of degree $p+1$ in the x and y directions, respectively, and a higher-order component. Prior to this, we need to establish the DGM orthogonality condition and prove two preliminary lemmas.

We begin by multiplying (2.1a) by $V \in \mathscr{V}_p$, integrating over the element Δ and using Green's formula to obtain

$$\int_{\Gamma} \boldsymbol{\alpha}\cdot\boldsymbol{v} V u \,\mathrm{d}\sigma - \iint_{\Delta} \boldsymbol{\alpha}\cdot\nabla V u \,\mathrm{d}x\,\mathrm{d}y = \iint_{\Delta} f(x,y) V \,\mathrm{d}x\,\mathrm{d}y. \tag{2.9}$$

Applying Green's formula to (2.5) leads to

$$\int_{\Gamma_{\text{out}}} \boldsymbol{\alpha}\cdot\boldsymbol{v} U V \,\mathrm{d}\sigma + \int_{\Gamma_{\text{in}}} \boldsymbol{\alpha}\cdot\boldsymbol{v} U^- V \,\mathrm{d}\sigma - \iint_{\Delta} \boldsymbol{\alpha}\cdot\nabla V U \,\mathrm{d}x\,\mathrm{d}y = \iint_{\Delta} f(x,y) V \,\mathrm{d}x\,\mathrm{d}y. \tag{2.10}$$

Subtracting (2.10) from (2.9) leads to the DGM orthogonality condition

$$\int_{\Gamma_{\text{in}}} \boldsymbol{\alpha}\cdot\boldsymbol{v}\epsilon^- V \,\mathrm{d}\sigma + \int_{\Gamma_{\text{out}}} \boldsymbol{\alpha}\cdot\boldsymbol{v}\epsilon V \,\mathrm{d}\sigma - \int_0^h\int_0^h \boldsymbol{\alpha}\cdot\nabla V \epsilon \,\mathrm{d}x\,\mathrm{d}y = 0, \quad \forall V \in \mathscr{V}_p, \tag{2.11}$$

where

$$\epsilon = u - U \tag{2.12}$$

is the local finite element discretization error. Using the mapping of $[0,h]^2$ onto the canonical element $[-1,1]^2$ defined by $x = h(1+\xi)/2$ and $y = h(1+\eta)/2$ and $\hat{u}(\xi,\eta) = u(x(\xi), y(\eta))$ we obtain the DGM orthogonality condition (2.11) on the canonical element

$$\int_{\hat{\Gamma}_{\text{in}}} \boldsymbol{\alpha}\cdot\boldsymbol{v}\hat{\epsilon}^- \hat{V} \,\mathrm{d}\hat{\sigma} + \int_{\hat{\Gamma}_{\text{out}}} \boldsymbol{\alpha}\cdot\boldsymbol{v}\hat{\epsilon}\hat{V} \,\mathrm{d}\hat{\sigma} - \int_{-1}^{1}\int_{-1}^{1} \boldsymbol{\alpha}\cdot\nabla\hat{V}\hat{\epsilon} \,\mathrm{d}\xi\,\mathrm{d}\eta = 0, \quad \forall \hat{V} \in \hat{\mathscr{V}}_p. \tag{2.13}$$

In the remainder of this paper we will omit the $\hat{}$ unless we feel it is needed for clarity.

Lemma 2.1. *If $Q_k \in \mathscr{V}_k$ satisfies*

$$\int_{\Gamma_{\text{out}}} \boldsymbol{\alpha}\cdot\boldsymbol{v} Q_k V \,\mathrm{d}\sigma - \iint_{\Delta} \boldsymbol{\alpha}\cdot\nabla V Q_k \,\mathrm{d}\xi\,\mathrm{d}\eta = 0, \quad \forall V \in \mathscr{V}_p,\ k \leqslant p, \tag{2.14}$$

then

$$Q_k = 0, \quad k \leqslant p. \tag{2.15}$$

Proof. Using Green's formula we write (2.14) as

$$-\int_{\Gamma_{\text{in}}} \boldsymbol{\alpha}\cdot\boldsymbol{v} Q_k V \,\mathrm{d}\sigma + \iint_{\Delta} \boldsymbol{\alpha}\cdot\nabla Q_k V \,\mathrm{d}\xi\,\mathrm{d}\eta = 0, \quad \forall V \in \mathscr{V}_p. \tag{2.16}$$

Adding (2.14) to (2.16) with $V = Q_k$ we obtain

$$-\int_{\Gamma_{\text{in}}} \boldsymbol{\alpha}\cdot\boldsymbol{\nu} Q_k^2\,\mathrm{d}\sigma + \int_{\Gamma_{\text{out}}} \boldsymbol{\alpha}\cdot\boldsymbol{\nu} Q_k^2\,\mathrm{d}\sigma = \int_{\Gamma} |\boldsymbol{\alpha}\cdot\boldsymbol{\nu}| Q_k^2\,\mathrm{d}\sigma = 0, \quad k \leqslant p. \tag{2.17}$$

This leads to $Q_k = 0$ on Γ. Combining this with (2.16) for $V = \boldsymbol{\alpha}\cdot\nabla Q_k$ yields $\boldsymbol{\alpha}\cdot\nabla Q_k = 0$ on Δ which completes the proof. □

In the following lemma we will write the interpolation error as a power series in h.

Lemma 2.2. *Let $w \in C^{\infty}(0,h)$ and πw be a p-degree polynomial that interpolates w at Radau points on $[0,h]$. Then the interpolation error*

$$w(x(\xi)) - \pi w(x(\xi)) = \sum_{k=p+1}^{\infty} Q_k^-(\xi) h^k, \tag{2.18}$$

where

$$Q_{p+1}^-(\xi) = \frac{w^{(p+1)}(0)}{2^{p+1}(p+1)!}(\xi-\xi_0)(\xi-\xi_1)\cdots(\xi-\xi_p) = c_{p+1}R_{p+1}(\xi) \tag{2.19}$$

and

$$Q_k^-(\xi) = R_{p+1}(\xi) r_{k-p-1}(\xi), \quad k > p+1, \tag{2.20}$$

with $r_k(\xi)$ being a polynomial of degree k.

Proof. By the standard interpolation error there exists $s(x)$ such that

$$w(x) - \pi w(x) = \frac{w^{(p+1)}(s(x,h))}{(p+1)!}(x-x_0)(x-x_1)\cdots(x-x_p), \quad x \in [0,h], \tag{2.21}$$

where $x_i = h(1+\xi_i)/2$ and ξ_i, $i = 0,1,\ldots,p$, are the roots of right Radau polynomial R_{p+1} in $[-1,1]$. On $[-1,1]$ the interpolation error can be written as

$$w(\xi) - \pi w(\xi) = \frac{h^{p+1} w^{(p+1)}(s(x(\xi),h))}{2^{p+1}(p+1)!}(\xi-\xi_0)(\xi-\xi_1)\cdots(\xi-\xi_p), \quad \xi \in [-1,1]. \tag{2.22}$$

The Maclaurin series of $w^{(p+1)}(s(x(\xi),h))$ with respect to h yields

$$w^{(p+1)}(s(x(\xi),h)) = w^{(p+1)}(0) + \sum_{k=1}^{\infty} h^k q_k(\xi), \tag{2.23a}$$

where

$$q_k(\xi) = \frac{1}{k!}\left.\frac{\mathrm{d}^k w^{(p+1)}(s(x(\xi),h))}{\mathrm{d}h^k}\right|_{h=0}, \quad k > 0 \tag{2.23b}$$

is a polynomial of degree k.

Combining (2.22), (2.23a) and (2.23b) completes the proof. □

Now we are ready to state the main result of this section.

Theorem 2.1. *Let u and U be the solution of* (2.1a), (2.1b) *and* (2.5), *respectively. Then the local finite element error can be written as*

$$\epsilon(\xi,\eta)=\sum_{k=p+1}^{\infty}h^k Q_k(\xi,\eta), \tag{2.24}$$

where

$$Q_{p+1}=\beta_1 R_{p+1}(\xi)+\beta_2 R_{p+1}(\eta). \tag{2.25}$$

Furthermore, at the outflow boundary of the physical element Δ

$$\int_{\Gamma_{\text{out}}}\boldsymbol{\alpha}\cdot\boldsymbol{\nu}\epsilon\,\mathrm{d}\sigma=\mathrm{O}(h^{2p+2}). \tag{2.26}$$

Proof. Writing the Maclaurin series of the local error ϵ with respect to h yields

$$\epsilon=\sum_{k=0}^{\infty}Q_k(\xi,\eta)h^k. \tag{2.27}$$

Substituting the series (2.27) in the DGM orthogonality condition (2.13), using (2.18) and collecting terms having the same powers of h we write

$$\begin{aligned}&\sum_{k=0}^{p}h^k\left(\int_{\Gamma_{\text{out}}}\boldsymbol{\alpha}\cdot\boldsymbol{\nu}Q_kV\,\mathrm{d}\sigma-\iint_{\Delta}\boldsymbol{\alpha}\cdot\nabla VQ_k\,\mathrm{d}\xi\,\mathrm{d}\eta\right)\\&\quad+\sum_{k=p+1}^{\infty}h^k\left(\int_{\Gamma_{\text{in}}}\boldsymbol{\alpha}\cdot\boldsymbol{\nu}Q_k^{-}V\,\mathrm{d}\sigma+\int_{\Gamma_{\text{out}}}\boldsymbol{\alpha}\cdot\boldsymbol{\nu}Q_kV\,\mathrm{d}\sigma-\iint_{\Delta}\boldsymbol{\alpha}\cdot\nabla VQ_k\,\mathrm{d}\xi\,\mathrm{d}\eta\right)=0,\quad\forall V\in\mathscr{V}_p.\end{aligned} \tag{2.28}$$

Thus, for $0\leqslant k\leqslant p$ we have

$$\int_{\Gamma_{\text{out}}}\boldsymbol{\alpha}\cdot\boldsymbol{\nu}Q_kV\,\mathrm{d}\sigma-\iint_{\Delta}\boldsymbol{\alpha}\cdot\nabla VQ_k\,\mathrm{d}\xi\,\mathrm{d}\eta=0,\quad\forall V\in\mathscr{V}_p. \tag{2.29}$$

By Lemma 2.1, (2.29) leads to $Q_k=0$, $k=0,1,\ldots,p$, and establishes (2.24).

On the other-hand, using Lemma 2.2, we write

$$Q_{p+1}^{-}(\xi,\eta)=\begin{cases}\dfrac{1}{2^{p+1}(p+1)!}\dfrac{\partial^{p+1}u}{\partial x^{p+1}}(0,0)(\xi-\xi_0)(\xi-\xi_1)\cdots(\xi-\xi_p) & \text{on } \Gamma_1,\\ \dfrac{1}{2^{p+1}(p+1)!}\dfrac{\partial^{p+1}u}{\partial y^{p+1}}(0,0)(\eta-\xi_0)(\eta-\xi_1)\cdots(\eta-\xi_p) & \text{on } \Gamma_4.\end{cases} \tag{2.30}$$

A direct computation reveals that Q_{p+1} can be split as

$$Q_{p+1}=\frac{1}{(p+1)!}\frac{\mathrm{d}^{p+1}(u-U)}{\mathrm{d}h^{p+1}}(\xi,\eta)\bigg|_{h=0}=\check{Q}_{p+1}+\tilde{Q}_p, \tag{2.31a}$$

where $\tilde{Q}_p(\xi,\eta)\in\mathscr{V}_p$ and

$$\begin{aligned}\check{Q}_{p+1}=&\frac{1}{2^{p+1}(p+1)!}\frac{\partial^{p+1}u}{\partial x^{p+1}}(0,0)(\xi-\xi_0)(\xi-\xi_1)\cdots(\xi-\xi_p)\\&+\frac{1}{2^{p+1}(p+1)!}\frac{\partial^{p+1}u}{\partial y^{p+1}}(0,0)(\eta-\xi_0)(\eta-\xi_1)\cdots(\eta-\xi_p).\end{aligned} \tag{2.31b}$$

Substituting (2.31a) and (2.31b) in the $O(h^{p+1})$ term of the series (2.28) leads to

$$\int_{\Gamma_{\text{in}}} \boldsymbol{\alpha}\cdot\boldsymbol{\nu} Q_{p+1}^{-} V \,\mathrm{d}\sigma + \int_{\Gamma_{\text{out}}} \boldsymbol{\alpha}\cdot\boldsymbol{\nu}\check{Q}_{p+1} V \,\mathrm{d}\sigma - \iint_{\Delta} \boldsymbol{\alpha}\cdot\nabla V \check{Q}_{p+1}\,\mathrm{d}\xi\,\mathrm{d}\eta + \int_{\Gamma_{\text{out}}} \boldsymbol{\alpha}\cdot\boldsymbol{\nu}\tilde{Q}_p V \,\mathrm{d}\sigma - \iint_{\Delta} \boldsymbol{\alpha}\cdot\nabla V \tilde{Q}_p\,\mathrm{d}\xi\,\mathrm{d}\eta = 0, \quad \forall V \in \mathscr{V}_p. \tag{2.32}$$

Using (2.30) and (2.31b) we can show that

$$\int_{\Gamma_{\text{in}}} \boldsymbol{\alpha}\cdot\boldsymbol{\nu} Q_{p+1}^{-} V \,\mathrm{d}\sigma + \int_{\Gamma_{\text{out}}} \boldsymbol{\alpha}\cdot\boldsymbol{\nu}\check{Q}_{p+1} V \,\mathrm{d}\sigma - \iint_{\Delta} \boldsymbol{\alpha}\cdot\nabla V \check{Q}_{p+1}\,\mathrm{d}\xi\,\mathrm{d}\eta = 0, \quad \forall V \in \mathscr{V}_p. \tag{2.33}$$

Combining (2.32) and (2.33) with Lemma 2.1 leads to $\tilde{Q}_p = 0$. Using (2.31a) and (2.31b) we establish (2.25).

Using (2.30) with Lemma 2.2 we can show that

$$\int_{\Gamma_{\text{in}}} \boldsymbol{\alpha}\cdot\boldsymbol{\nu} Q_k^{-} V \,\mathrm{d}\sigma = 0, \quad \forall V \in \mathscr{V}_{2p-k},\ k = p+1,\ldots,2p. \tag{2.34}$$

Using (2.34), the $O(h^k)$, $p+1 \leqslant k \leqslant 2p$, term of (2.28) yields

$$\int_{\Gamma_{\text{out}}} \boldsymbol{\alpha}\cdot\boldsymbol{\nu} Q_k V \,\mathrm{d}\sigma - \iint_{\Delta} \boldsymbol{\alpha}\cdot\nabla V Q_k\,\mathrm{d}\xi\,\mathrm{d}\eta = 0, \quad \forall V \in \mathscr{V}_{2p-k}. \tag{2.35}$$

Testing against $V = 1$ we obtain

$$\int_{\Gamma_{\text{out}}} \boldsymbol{\alpha}\cdot\boldsymbol{\nu} Q_k \,\mathrm{d}\sigma = 0, \quad k = p+1,\ldots,2p \tag{2.36}$$

which establishes (2.26). □

In the previous theorem we have extended the results of Adjerid et al. [1] to multi-dimensional problems on square meshes. In particular, we have proved that the p-degree DG solution is $O(h^{p+2})$ superconvergent at Radau points (ξ_i, ξ_j), $i,j = 0,\ldots,p$ and that the DG solution has an $O(h^{2p+2})$ superconvergence on average at the outflow boundary of Δ.

We note that for an arbitrary nonzero constant vector $\boldsymbol{\alpha}$, (2.24)–(2.26) hold where the significant part of the error is spanned by the $p+1$-degree Radau polynomials

$$R_{p+1}(\xi) = L_{p+1}(\xi) - \operatorname{sign}(\alpha_1) L_p(\xi), \qquad R_{p+1}(\eta) = L_{p+1}(\eta) - \operatorname{sign}(\alpha_2) L_p(\eta). \tag{2.37}$$

2.1. Global error analysis

In the following theorem we will show a superconvergence result for the global discretization error if $p \geqslant 1$.

Theorem 2.2. *Under the conditions of Theorem* 2.1 *the global finite element error e for $p \geqslant 1$ satisfies the superconvergence result*

$$\int_{\Omega_{\text{out}}} \boldsymbol{\alpha}\cdot\boldsymbol{\nu} e(x,y)\,\mathrm{d}\sigma = O(h^{2p+1}). \tag{2.38}$$

Proof. Adding and subtracting $u(x,y)$ to both terms on the left side of (2.5) we obtain

$$\int_{\Gamma_{\text{in}}} \boldsymbol{\alpha}\cdot\boldsymbol{\nu} V(U^- - u + u - U)\,\mathrm{d}\sigma + \iint_{\Delta} \boldsymbol{\alpha}\cdot\nabla(U-u+u)V\,\mathrm{d}x\,\mathrm{d}y = \iint_{\Delta} f(x,y)V\,\mathrm{d}x\,\mathrm{d}y, \quad \forall V \in \mathscr{V}_p, \tag{2.39}$$

where Δ is an arbitrary element.

This can be written as

$$\int_{\Gamma_{\text{in}}} \boldsymbol{\alpha}\cdot\boldsymbol{\nu} V(e - e^-)\,\mathrm{d}\sigma - \iint_{\Delta} \boldsymbol{\alpha}\cdot\nabla eV\,\mathrm{d}x\,\mathrm{d}y = 0 \quad \forall V \in \mathscr{V}_p. \tag{2.40}$$

Integrating by parts leads to

$$\int_{\Gamma_{\text{in}}} \boldsymbol{\alpha}\cdot\boldsymbol{\nu} Ve^-\,\mathrm{d}\sigma + \int_{\Gamma_{\text{out}}} \boldsymbol{\alpha}\cdot\boldsymbol{\nu} Ve\,\mathrm{d}\sigma - \iint_{\Delta} \boldsymbol{\alpha}\cdot\nabla Ve\,\mathrm{d}x\,\mathrm{d}y = 0 \quad \forall V \in \mathscr{V}_p. \tag{2.41}$$

Testing against $V = 1$ yields

$$\int_{\Gamma_{\text{in}}} \boldsymbol{\alpha}\cdot\boldsymbol{\nu} e^-\,\mathrm{d}\sigma + \int_{\Gamma_{\text{out}}} \boldsymbol{\alpha}\cdot\boldsymbol{\nu} e\,\mathrm{d}\sigma = 0. \tag{2.42}$$

Summing over all elements we obtain

$$\int_{\Omega_{\text{in}}} \boldsymbol{\alpha}\cdot\boldsymbol{\nu} e^-\,\mathrm{d}\sigma + \int_{\Omega_{\text{out}}} \boldsymbol{\alpha}\cdot\boldsymbol{\nu} e\,\mathrm{d}\sigma = 0. \tag{2.43}$$

Combining (2.43) and Lemma 2.2 we establish (2.38). □

2.2. Nonlinear problems

We will describe similar results for problems of the form

$$\boldsymbol{\alpha}\cdot\nabla u + \phi(u) = f(x,y), \quad (x,y) \in \Omega \tag{2.44}$$

with boundary conditions at the inflow boundary.

The DGM weak formulation consists of determining $U(x,y) \in \mathscr{V}_p$ on Δ such that

$$\int_{\Gamma_{\text{in}}} \boldsymbol{\alpha}\cdot\boldsymbol{\nu} V(U^- - U)\,\mathrm{d}\sigma + \iint_{\Delta} [\boldsymbol{\alpha}\cdot\nabla UV + \phi(U)V]\,\mathrm{d}x\,\mathrm{d}y = \iint_{\Delta} f(x,y)V\,\mathrm{d}x\,\mathrm{d}y, \quad \forall V \in \mathscr{V}_p. \tag{2.45}$$

In the following theorem we state superconvergence results and local error estimates for nonlinear problems.

Theorem 2.3. *Let u and U be the solution of* (2.44) *and* (2.45), *respectively. If u is smooth, then the local error estimates* (2.24) *and* (2.25) *hold.*

Proof. The DGM orthogonality for (2.44) on an element Δ can be written as

$$\int_{\Gamma_{\text{in}}} \boldsymbol{\alpha}\cdot\boldsymbol{\nu}\epsilon^- V\,\mathrm{d}\sigma + \int_{\Gamma_{\text{out}}} \boldsymbol{\alpha}\cdot\boldsymbol{\nu}\epsilon V\,\mathrm{d}\sigma - \int_0^h \int_0^h [\boldsymbol{\alpha}\cdot\nabla V\epsilon + (\phi(u) - \phi(U))V]\,\mathrm{d}x\,\mathrm{d}y = 0, \quad \forall V \in \mathscr{V}_p. \tag{2.46}$$

On $[-1,1]\times[-1,1]$ the orthogonality condition (2.46) becomes

$$\int_{\Gamma_{\text{in}}} \boldsymbol{\alpha}\cdot\boldsymbol{\nu}\epsilon^{-}V\,\mathrm{d}\sigma+\int_{\Gamma_{\text{out}}} \boldsymbol{\alpha}\cdot\boldsymbol{\nu}\epsilon V\,\mathrm{d}\sigma-\int_{-1}^{1}\int_{-1}^{1}\left[\boldsymbol{\alpha}\cdot\nabla V\epsilon+\frac{h}{2}(\phi(u)-\phi(U))V\right]\mathrm{d}\xi\,\mathrm{d}\eta=0,\quad \forall V\in\mathscr{V}_p. \tag{2.47}$$

Assuming ϕ analytic and ϕ'' bounded and using Taylor series of ϕ about u we have

$$\phi(u)-\phi(U)=a(u)\epsilon-\frac{\epsilon^2}{2}\phi''(\bar{u}),\quad a(u)=\phi'(u). \tag{2.48a}$$

The Maclaurin series of $a(u)$ with respect to h yields

$$a(u)=2\sum_{k=0}^{\infty}h^k\overline{Q}_k(\xi,\eta),\qquad \overline{Q}_k(\xi,\eta)=\frac{1}{2}\frac{\phi^{(k+1)}(u(x(\xi),y(\eta)))}{k!}\frac{\mathrm{d}^k u}{\mathrm{d}h^k}(x(\xi),y(\eta))|_{h=0}\in\mathscr{P}_k. \tag{2.48b}$$

We note that in order to establish (2.48b) we used the chain rule with $x(\xi)=h(1+\xi)/2$ and $y(\eta)=h(1+\eta)/2$.

Substituting (2.27), (2.48a) and (2.48b) in (2.47) and collecting terms having same powers of h lead to

$$\begin{aligned}&\int_{\Gamma_{\text{out}}}\boldsymbol{\alpha}\cdot\boldsymbol{\nu}Q_0V\,\mathrm{d}\sigma-\iint_{\Delta}\boldsymbol{\alpha}\cdot\nabla VQ_0\,\mathrm{d}\xi\,\mathrm{d}\eta+\sum_{k=1}^{p}h^k\left(\int_{\Gamma_{\text{out}}}\boldsymbol{\alpha}\cdot\boldsymbol{\nu}Q_kV\,\mathrm{d}\sigma-\iint_{\Delta}[\boldsymbol{\alpha}\cdot\nabla VQ_k+Z_{k-1}V]\,\mathrm{d}\xi\,\mathrm{d}\eta\right)\\&+\sum_{k=p+1}^{\infty}h^k\left(\int_{\Gamma_{\text{in}}}\boldsymbol{\alpha}\cdot\boldsymbol{\nu}Q_k^{-}V\,\mathrm{d}\sigma+\int_{\Gamma_{\text{out}}}\boldsymbol{\alpha}\cdot\boldsymbol{\nu}Q_kV\,\mathrm{d}\sigma-\iint_{\Delta}[\boldsymbol{\alpha}\cdot\nabla VQ_k+Z_{k-1}V]\,\mathrm{d}\xi\,\mathrm{d}\eta\right)=0,\quad\forall V\in\mathscr{V}_p,\end{aligned} \tag{2.49a}$$

where

$$Z_k=\sum_{l=0}^{k}\overline{Q}_lQ_{k-l}. \tag{2.49b}$$

Applying Lemma 2.2, the O(1) term yields $Q_0=0$. By induction we prove that $Q_k=0$, $k=0,1,\ldots,p$. We note that the term in (2.48a) involving ϵ^2 is higher order and does not contribute to our leading terms.

Following the same lines of reasoning used to prove (2.25) we establish the same result for nonlinear problems. □

3. A posteriori error estimation

The results of Theorem 2.1 and 2.2 suggest that the global finite element error on each element Δ can be approximated as

$$e(x,y)=u-U\approx E(x,y)=b_1R_{p+1}(x)+b_2R_{p+1}(y). \tag{3.1}$$

Substituting u in (2.5) by $e+U$ leads to

$$\iint_{\Delta}\boldsymbol{\alpha}\cdot\nabla(U+e)W\,\mathrm{d}x\,\mathrm{d}y=\iint_{\Delta}fW\,\mathrm{d}x\,\mathrm{d}y. \tag{3.2}$$

Approximating e by E yields the following discrete problem for the error

$$\iint_{\Delta}\boldsymbol{\alpha}\cdot\nabla(U+E)R_{p+1}(x)\,\mathrm{d}x\,\mathrm{d}y=\iint_{\Delta}fR_{p+1}(x)\,\mathrm{d}x\,\mathrm{d}y, \tag{3.3a}$$

$$\iint_{\Delta} \boldsymbol{\alpha} \cdot \nabla(U+E)R_{p+1}(y)\,\mathrm{d}x\,\mathrm{d}y = \iint_{\Delta} fR_{p+1}(y)\,\mathrm{d}x\,\mathrm{d}y. \tag{3.3b}$$

We note that the strong superconvergence (2.26) of p-degree, $p > 0$, finite element solution flux at the outflow boundary of each element suggests that we should neglect the jump terms in the error problem without compromising the accuracy of our error estimate. Since for $p = 0$ this strong superconvergence at the outflow boundary is lost and (3.3a) and (3.3b) fails to have a unique solution, we solve the following problem for the error estimate

$$\int_{\Gamma_{\mathrm{in}}} \boldsymbol{\alpha} \cdot \boldsymbol{\nu}(U^- + E^- - U - E)R_1(x)\,\mathrm{d}\sigma + \iint_{\Delta} \boldsymbol{\alpha} \cdot \nabla(U+E)R_1(x)\,\mathrm{d}x\,\mathrm{d}y = \iint_{\Delta} fR_1(x)\,\mathrm{d}x\,\mathrm{d}y, \tag{3.4a}$$

$$\int_{\Gamma_{\mathrm{in}}} \boldsymbol{\alpha} \cdot \boldsymbol{\nu}(U^- + E^- - U - E)R_1(y)\,\mathrm{d}\sigma + \iint_{\Delta} \boldsymbol{\alpha} \cdot \nabla(U+E)R_1(y)\,\mathrm{d}x\,\mathrm{d}y = \iint_{\Delta} fR_1(y)\,\mathrm{d}x\,\mathrm{d}y. \tag{3.4b}$$

For nonlinear problems of the form

$$u_y + h(u)_x = f(x,y) \tag{3.5}$$

we find E by solving the linearized problem

$$\iint_{\Delta} [h'(U),1] \cdot \nabla(U+E)R_{p+1}(x)\,\mathrm{d}x\,\mathrm{d}y = \iint_{\Delta} fR_{p+1}(x)\,\mathrm{d}x\,\mathrm{d}y, \tag{3.6a}$$

$$\iint_{\Delta} [h'(U),1] \cdot \nabla(U+E)R_{p+1}(y)\,\mathrm{d}x\,\mathrm{d}y = \iint_{\Delta} fR_{p+1}(y)\,\mathrm{d}x\,\mathrm{d}y. \tag{3.6b}$$

We also use the solution of the linearized problem (3.6a) and (3.6b) as an initial guess for Newton iteration when solving the nonlinear finite element problem for E

$$\iint_{\Delta} [h'(U+E),1] \cdot \nabla(U+E)R_{p+1}(x)\,\mathrm{d}x\,\mathrm{d}y = \iint_{\Delta} fR_{p+1}(x)\,\mathrm{d}x\,\mathrm{d}y, \tag{3.7a}$$

$$\iint_{\Delta} [h'(U+E),1] \cdot \nabla(U+E)R_{p+1}(y)\,\mathrm{d}x\,\mathrm{d}y = \iint_{\Delta} fR_{p+1}(y)\,\mathrm{d}x\,\mathrm{d}y. \tag{3.7b}$$

An accepted efficiency measure of a posteriori error estimates is the effectivity index. In this paper we use the local effectivity indices in the $\mathscr{L}^2$ norm

$$\theta_i = \frac{\|E\|_{\mathscr{L}^2(\Delta_i)}}{\|e\|_{\mathscr{L}^2(\Delta_i)}}, \quad i = 1,2,\ldots,N \tag{3.8}$$

and the global effectivity index

$$\theta = \frac{\|E\|_{\mathscr{L}^2(\Omega)}}{\|e\|_{\mathscr{L}^2(\Omega)}}. \tag{3.9}$$

Ideally, effectivity indices should approach unity under mesh refinement.

4. Numerical examples

Example 1. We consider the linear hyperbolic problem

$$u_x + 2u_y = f(x,y), \qquad (x,y) \in [0,1]^2 \tag{4.1a}$$

subject to the boundary conditions

$$u(x,0) = g_0(x) \qquad u(0,y) = g_1(y). \tag{4.1b}$$

We select $f(x,y)$, g_0 and g_1 such that the exact solution is

$$u(x,y) = \mathrm{e}^{x+y}. \tag{4.1c}$$

We perform several tests on this example to study the effect of boundary conditions on the quality of our a posteriori error estimates and show the superconvergence points of the discontinuous Galerkin solution.

We start by solving (4.1a)–(4.1c) on a uniform mesh having 64 elements with $p = 1, 2, 3$ with U^- being the true boundary conditions. We repeat the previous experiment with U^- being the interpolant of true boundary conditions at Radau points as defined in (2.6). We present the local effectivity indices in Figs. 2 and 3. The effectivity indices corresponding to the exact boundary conditions are farther from unity than those corresponding to interpolated boundary conditions, especially on elements near the inflow boundaries. In both experiments the effectivity indices converge to one under p refinement.

We solve (4.1a)–(4.1c) using U^- defined in (2.6) on a 16-element uniform mesh with p ranging from 1 to 6 and show the zero-level curves of the true error on each element in Fig. 4. As predicted by the theory of Section 2, these results indicate that the p-degree discontinuous Galerkin solution is superconvergent at Radau points, shown by 'x', on each element for $p \geqslant 1$.

Since there is no superconvergence for global errors when $p = 0$, the error estimation procedures (3.3a), (3.3b), (3.6a), (3.6b), (3.7a) and (3.7b) do not apply. This is illustrated by solving (4.1a), (4.1b), (4.1c), (3.4a) and (3.4b) using approximate boundary conditions on a 100-element mesh with $p = 0$ and presenting the local effectivity indices in Fig. 5. In this case we observe that the local effectivity indices get larger than unity away from the inflow boundary elements.

As a final test, we solve (4.1a)–(4.1c) on uniform meshes having 25, 100, 225, 400, 625 and 900 elements with $p = 1, 2, 3, 4$ using the true boundary conditions. We present the true errors in Table 1 and the global effectivity indices in Table 2. We repeat the previous experiment using approximate boundary conditions (2.6) with all other parameters unchanged and present the errors and global effectivity indices in Tables 3 and 4, respectively. The computational results indicate that the error estimates obtained using the procedure (3.3a) and (3.3b) converge to the true error under both h and p refinements. This is the first a posteriori finite element error estimate that exhibits convergence under h- and p-refinement for multi-dimensional problems. Since the effect of the true versus approximate boundary conditions on the effectivity indices is negligible, we shall use the approximate boundary conditions in the remainder of this section.

Example 2. We solve (4.1a)–(4.1c) on the quadrilateral domain $\Omega = ABCD$ where $A = (0,0)$, $B = (1,0.1)$, $C = (1,1)$ and $D = (1,1.1)$, on a 16-element mesh for $p = 1$–4 and show the zero levels of the contour plot of the error on each element in Fig. 6. The computational results suggest that the DG solution is superconvergent at the Radau points on more general meshes.

To show the convergence of our a posteriori error estimates under mesh refinement, we solve the previous problem on meshes having 25, 100, 225, 400, 625, 900 elements and $p = 1$–4. We present the effectivity indices in Table 5 which indicate that the error estimates converge to the true errors under both h and p refinements for quadrilateral meshes.

Example 3. We consider the following problem with a contact discontinuity

$$u_x + 2u_y = 0, \quad (x,y) \in [0,1]^2 \tag{4.2a}$$

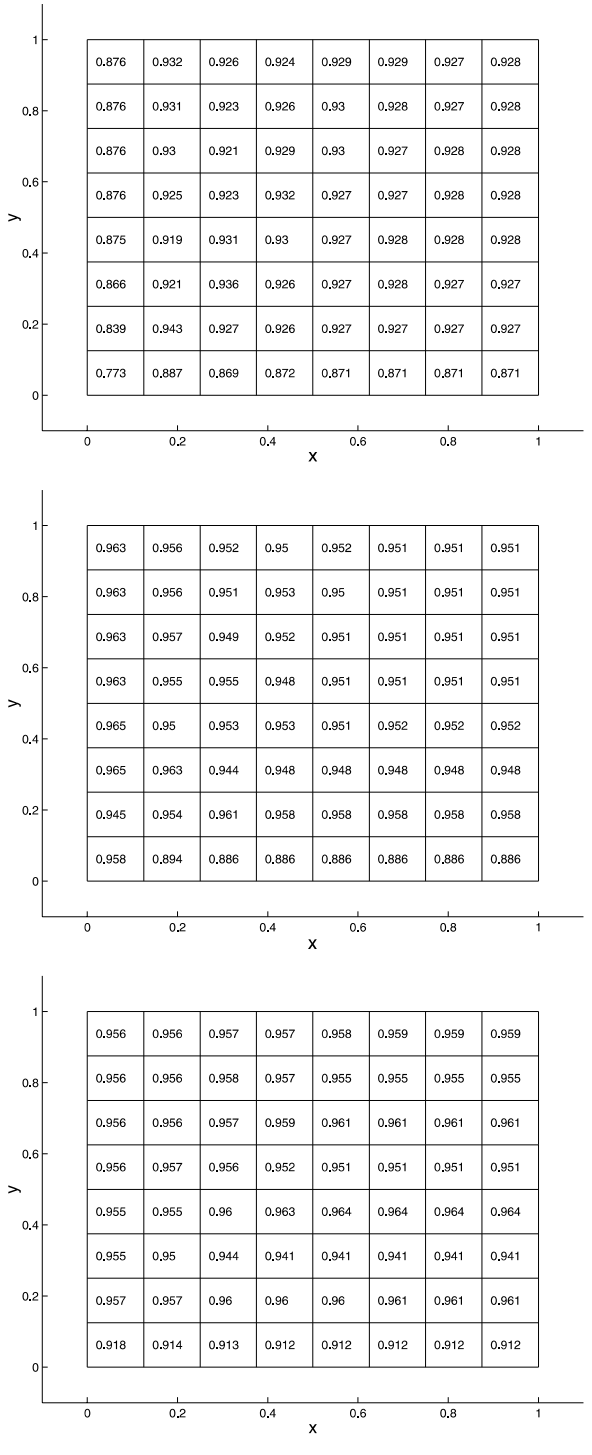

Fig. 2. Local effectivity indices for Example 1 on a 64-element uniform mesh and $p = 1, 2, 3$ (top to bottom) with true boundary conditions.

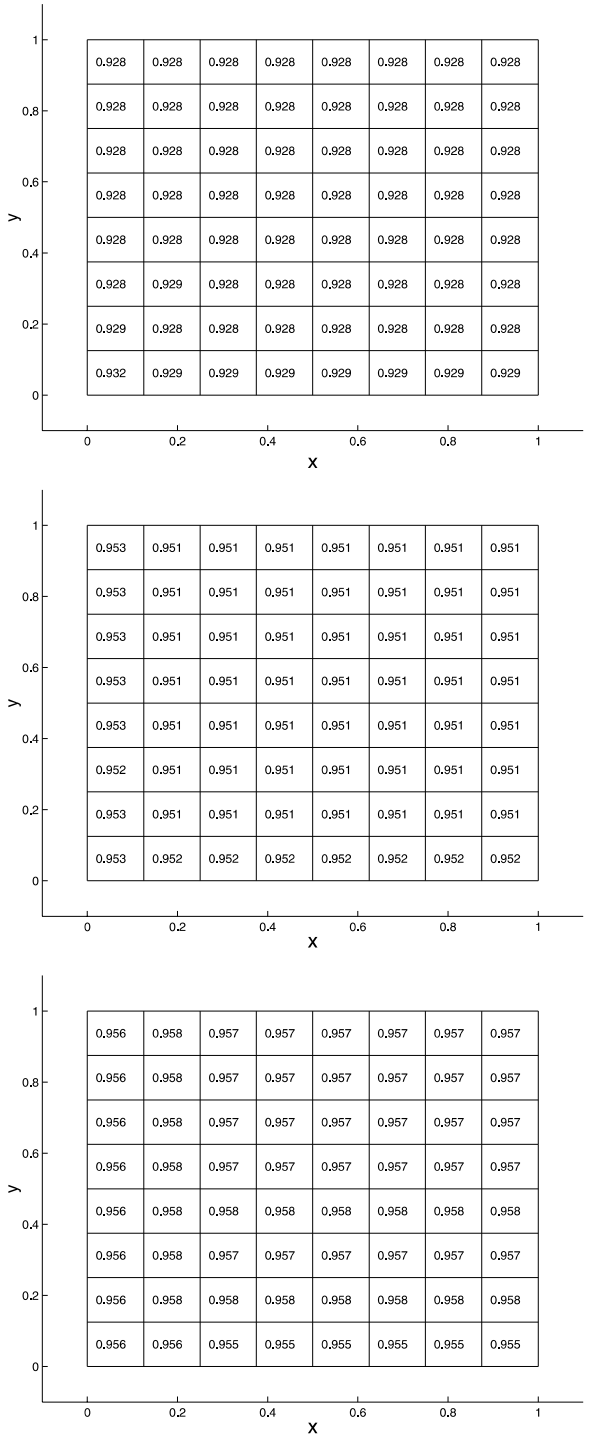

Fig. 3. Local effectivity indices for Example 1 on a 64-element uniform mesh and $p = 1, 2, 3$ (top to bottom) with approximate boundary conditions.

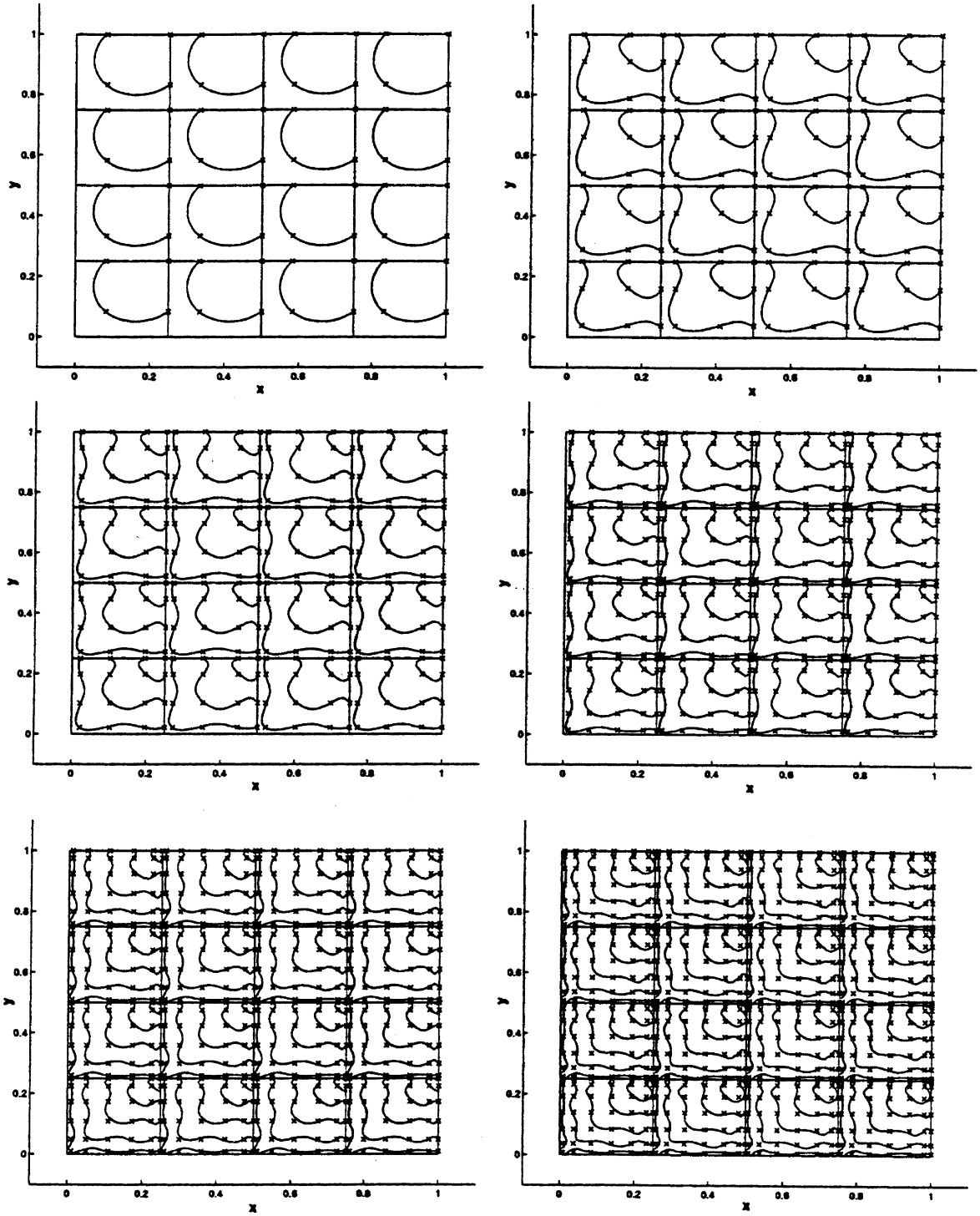

Fig. 4. Zero-level curves of the contour plot of the DG error for Example 1 on a 16-element uniform mesh and $p = 1$–6 (upper left to lower right) with approximate boundary conditions. Radau points are shown with an 'x'.

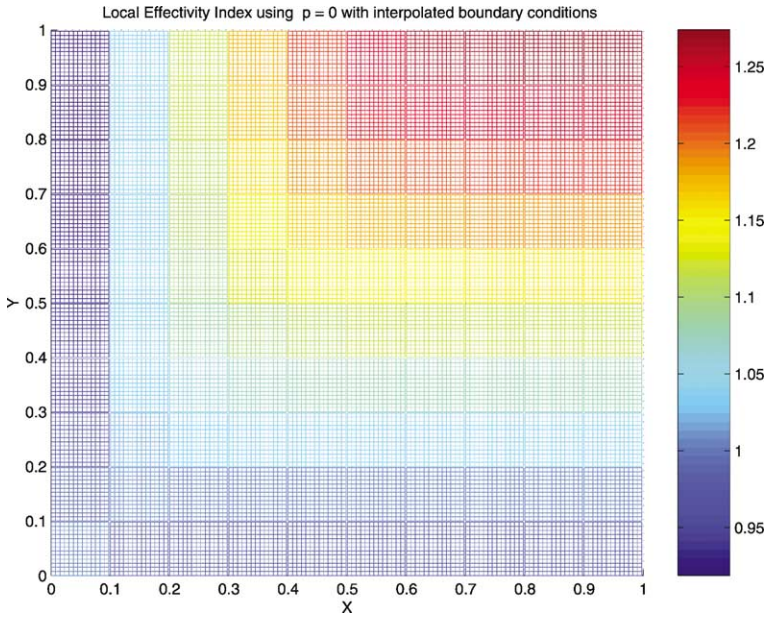

Fig. 5. Local effectivity indices for Example 1 on a 100-element uniform mesh for $p = 0$ with approximate boundary conditions.

Table 1
$\|e\|_{\mathscr{L}_2(\Omega)}$ for Example 1 on uniform meshes having 25, 100, 225, 400, 625, 900 elements and $p = 1$–4 with true boundary conditions

N	$p = 1$	$p = 2$	$p = 3$	$p = 4$
25	1.8684e−2	3.5066e−4	4.8726e−6	5.3577e−08
100	4.7156e−3	4.3948e−5	3.0338e−7	1.6526e−09
225	2.1027e−3	1.3035e−5	5.9883e−8	2.1708e−10
400	1.1847e−3	5.5019e−6	1.8943e−8	5.1475e−11
625	7.5894e−4	2.8179e−6	7.7583e−9	1.6860e−11
900	5.2738e−4	1.6311e−6	3.7413e−9	6.7745e−12

Table 2
Effectivity indices for Example 1 on uniform meshes having 25, 100, 225, 400, 625, 900 elements and $p = 1$–4 with true boundary conditions

N	$p = 1$	$p = 2$	$p = 3$	$p = 4$
25	0.8760	0.9188	0.9240	0.9236
100	0.9388	0.9597	0.9641	0.9659
225	0.9594	0.9732	0.9764	0.9781
400	0.9696	0.9800	0.9825	0.9839
625	0.9757	0.9840	0.9861	0.9872
900	0.9798	0.9867	0.9885	0.9894

Table 3
$\|e\|_{\mathscr{L}_2(\Omega)}$ for Example 1 on uniform meshes having 25, 100, 225, 400, 625, 900 elements and $p = 1$–4 with approximate boundary conditions

N	$p = 1$	$p = 2$	$p = 3$	$p = 4$
25	1.8793e−2	3.5112e−4	4.8676e−6	5.3588e−08
100	4.7299e−3	4.3971e−5	3.0306e−7	1.6514e−09
225	2.1069e−3	1.3039e−5	5.9836e−8	2.1693e−10
400	1.1865e−3	5.5031e−6	1.8931e−8	5.1436e−11
625	7.5987e−4	2.8184e−6	7.7542e−9	1.6849e−11
900	5.2793e−4	1.6313e−6	3.7396e−9	6.7701e−12

Table 4
Effectivity indices for Example 1 on uniform meshes having 25, 100, 225, 400, 625, 900 elements and $p = 1$–4 with approximate boundary conditions

N	$p = 1$	$p = 2$	$p = 3$	$p = 4$
25	0.8845	0.9211	0.9285	0.9257
100	0.9423	0.9610	0.9664	0.9676
225	0.9616	0.9741	0.9782	0.9795
400	0.9712	0.9807	0.9838	0.9851
625	0.9770	0.9846	0.9872	0.9883
900	0.9808	0.9871	0.9894	0.9903

subject to the boundary conditions

$$u(x,0) = \mathrm{e}^{-2x}, \quad 0 \leqslant x \leqslant 1, \tag{4.2b}$$

$$u(0,y) = \mathrm{e}^{y} + 0.25, \quad 0 < y \leqslant 1. \tag{4.2c}$$

The exact solution is

$$u(x,y) = \begin{cases} \mathrm{e}^{-2x+y} + 0.25 & \text{if } x < y/2, \\ \mathrm{e}^{-2x+y} & \text{if } x \geqslant y/2. \end{cases} \tag{4.2d}$$

The true solution has a contact discontinuity along $y = 2x$. Therefore, the smoothness assumption of Theorem 2.1 is violated and as a result we expect the a posteriori error estimate to perform poorly near the discontinuity.

We solve (4.2a)–(4.2d) on meshes having 32×32 and 200×200 elements with $p = 1, 2$ and present the local effectivity indices in Fig. 7. These computational results indicate that the local effectivity indices on elements away from the discontinuity converge to unity under mesh refinement. Our error estimates perform poorly on elements near the discontinuity. Since we are not using limiting to suppress spurious oscillations near the discontinuity, the region around the discontinuity where the error is underestimated gets wider as p increases.

Example 4. We consider the inviscid Burger's equation

$$u_y + uu_x = f(x,y) \quad (x,y) \in [-1,1]^2 \tag{4.3a}$$

subject to the boundary conditions

$$u(x,0) = g_0(x), \quad \text{and} \quad u(y,0) = g_1(x). \tag{4.3b}$$

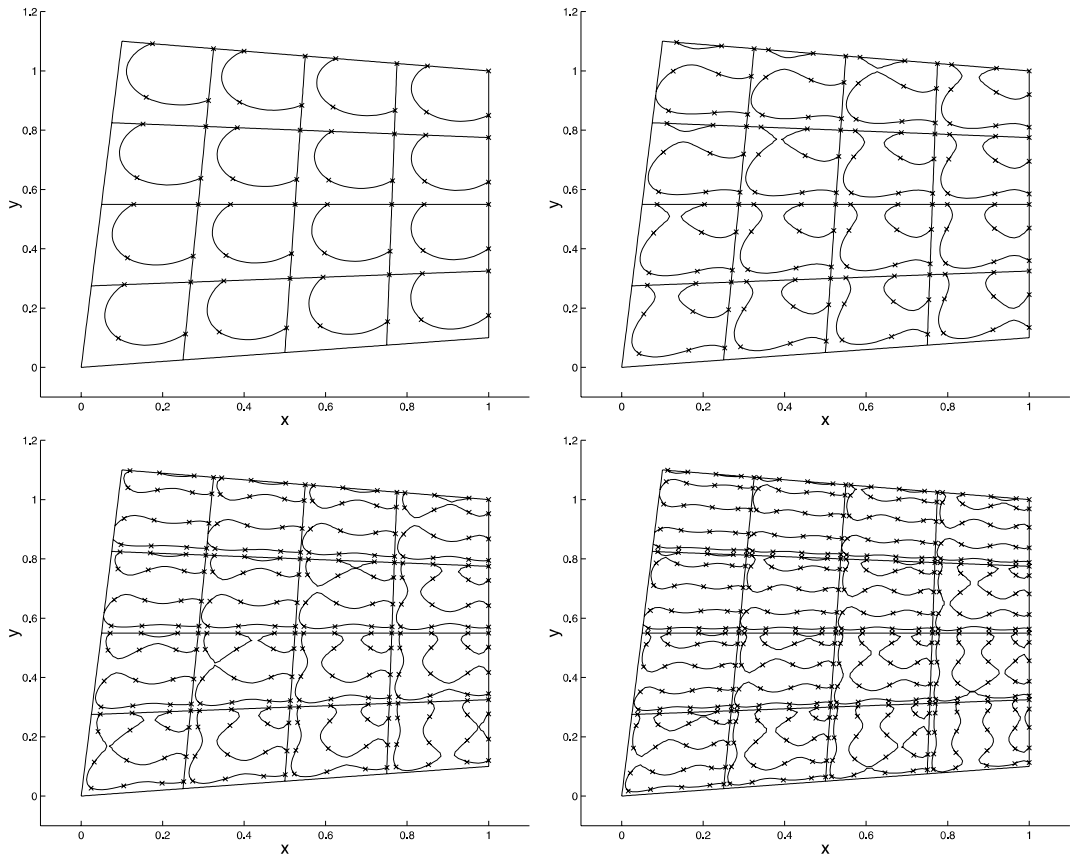

Fig. 6. Zero-level curves of the contour plot of the DG discretization error for Example 2 on a 16-element uniform mesh and $p = 1$–4 (upper left to lower right) with approximate boundary conditions. Radau points are shown with an 'x'.

Table 5
Global effectivity indices for Example 2 on uniform meshes having 25, 100, 225, 400, 625, 900 elements and $p = 1$–4

N	$p = 1$	$p = 2$	$p = 3$	$p = 4$
25	0.9416	0.9770	0.9901	0.9940
100	0.9707	0.9885	0.9951	0.9974
225	0.9804	0.9924	0.9968	0.9983
400	0.9853	0.9943	0.9976	0.9988
625	0.9882	0.9954	0.9981	0.9990
900	0.9902	0.9962	0.9984	0.9992

We select f, g_0 and g_1 such that the exact solution is

$$u(x,y) = \sqrt{1 + x^2 + 5y^2}. \tag{4.3c}$$

We solve (4.3a)–(4.3c) on meshes having 35, 140, 315, 560, 875, 1260, 1715 rectangular elements with an element aspect ratio $\Delta x/\Delta y = 5/7$ and $p = 1$–4, where Δx and Δy denote the length and width, respectively, of an element Δ. We compute a posteriori error estimates by solving the linear problem (3.6a) and (3.6b) and show the local effectivity indices in Table 6. We apply Newton's iteration to solve the nonlinear

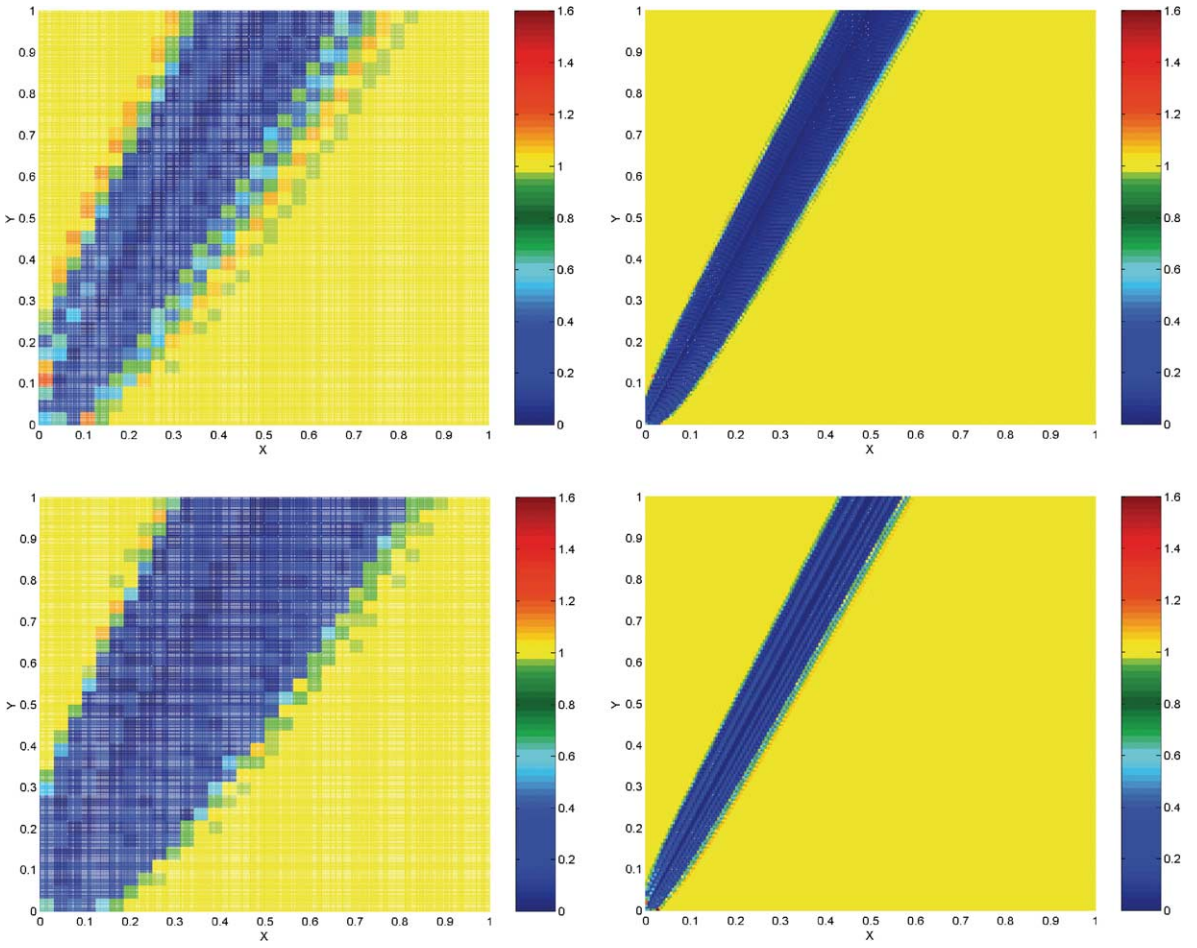

Fig. 7. Local effectivity indices for Example 3 with $(N,p) = (1024,1)$, $(40000,1)$, $(1024,2)$ and $(40000,2)$ (upper left to lower right).

Table 6
Effectivity indices Problem (4.3a)–(4.3c) using the linearized error estimator (3.6a) and (3.6b) on meshes having 35, 140, 315, 560, 875, 1260 and 1715 elements and $p = 1$–4

N	$p=1$	$p=2$	$p=3$	$p=4$
35	0.996059	1.003180	0.985678	1.287716
140	0.999087	0.998213	1.008134	1.003167
315	0.999579	0.999240	1.008920	1.008087
560	0.999761	0.999572	1.009565	1.008689
875	0.999847	0.999726	1.009887	1.008989
1260	0.999894	0.999810	1.010074	1.009149
1715	0.999922	0.999860	1.010191	1.009245

problem (3.7a) and (3.7b) using the linear error estimate (3.6a) and (3.6b) as an initial guess and present the effectivity indices in Table 7. While effectivity indices for both estimators are within 2% from unity, the error estimates obtained by solving the linear problem (3.6a) and (3.6b) are more efficient. For the remaining computational examples we will present numerical results for the linear error estimator only.

Table 7
Effectivity indices for problem (4.3a)–(4.3c) using the nonlinear error estimator (3.7a) and (3.7b) on meshes having 35, 140, 315, 560, 875, 1260, 1715 elements and $p = 1$–4

N	$p = 1$	$p = 2$	$p = 3$	$p = 4$
35	0.997489	1.004721	0.988137	1.280450
140	0.999433	0.998730	1.008672	1.003551
315	0.999733	0.999472	1.009163	1.008251
560	0.999848	0.999704	1.009703	1.008782
875	0.999902	0.999811	1.009975	1.009048
1260	0.999932	0.999869	1.010135	1.009190
1715	0.999950	0.999903	1.010236	1.009275

Table 8
Effectivity indices for homogeneous Burger's equation (4.3a) with initial condition (4.4) on $[-1,1] \times [0,0.4]$ using the linearized error estimate (3.6a) and (3.6b) on meshes having 35, 140, 315, 560, 875, 1260, 1680 elements and $p = 1$–4

N	$p = 1$	$p = 2$	$p = 3$	$p = 4$
35	0.9095	1.0698	0.7355	0.4947
140	1.0215	0.9184	0.7413	0.7246
315	0.9954	0.9443	0.9370	0.7349
560	1.0010	0.9851	0.9129	0.9487
875	1.0020	0.9832	0.9636	0.9269
1260	1.0025	0.9933	0.9680	0.9759
1680	0.9993	0.9866	0.9670	0.9770

Next we consider the homogeneous inviscid Burger's equation (4.3a) with $f(x,y) = 0$,

$$g_0(x,0) = 1 + \sin(\pi x)/2 \tag{4.4}$$

and select $g_1(0,y)$ such that the true solution is periodic and forms a shock discontinuity at the point $((2/\pi) - 1, (2/\pi))$ which propagates along $y = x + 1$. First, we solve this problem on $[-1,1] \times [0,0.4]$ with a smooth solution on meshes having 35, 140, 315, 560, 875, 1260, 1715 elements with an element aspect ratio $\Delta x/\Delta y = 25/7$ and $p = 1$–4. We compute an error estimate by solving (3.6a) and (3.6b) and present effectivity indices in Table 8. This example shows that the effectivity indices converge to one only under h refinement which is due to the steepening of the wave as the shock forms.

We conclude by solving the previous problem on $[-1,1] \times [0,1.999]$ on meshes having $N = 1260$ and 14 000 elements with an element aspect ratio $\Delta x/\Delta y = 7/5$ and $p = 1,2$. We plot the local effectivity indices in Fig. 8. These computational results indicate that the theoretical results of Theorem 2.1 are valid for nonlinear problems in regions where the solution is smooth, i.e., the local effectivity indices converge to unity under mesh refinement in regions where the solution is smooth. The regions in the lower right corner of the domain with underestimated errors correspond to regions of relatively small discretization errors and, thus, should not affect the quality of the global effectivity index.

5. Conclusion

We showed that the discontinuous Galerkin finite element error can be split into an $O(h^{p+1})$ leading component and a higher-order component. We further showed that the leading term is spanned by two $(p+1)$-degree Radau polynomials in the x and y directions, respectively. We used this result to construct an a posteriori estimate of the multi-dimensional discontinuous Galerkin finite element error for hyperbolic problems on rectangular meshes. The error estimation procedure is simple, can be computed in several

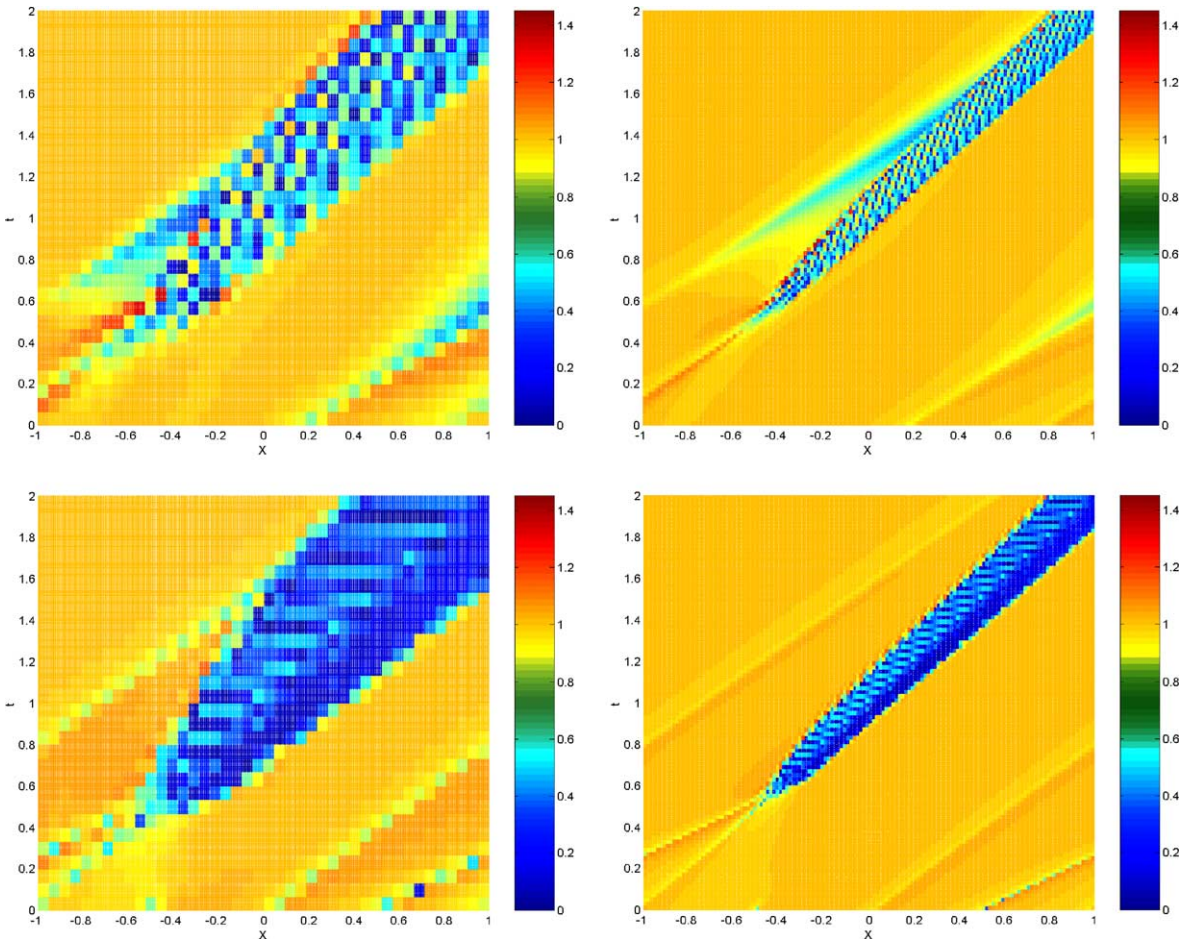

Fig. 8. Local effectivity indices for the homogeneous Burger's equation (4.3a) with initial condition (4.4) on $[-1,1]\times[0,1.999]$ using meshes having $(N,p)=(1260,1)$, $(14000,1)$, $(1260,2)$ and $(14000,2)$ (upper left to lower right).

norms and does not require any communication across neighboring elements. The later property makes this estimation procedure useful for parallel computations. The a posteriori error estimates developed in this paper readily extend to three-dimensional hexahedral elements. For a linear model problem we were able to show that the flux is strongly superconvergent on average on the outflow boundaries. This indicates that the error in the DGMs propagates at a higher order. Superconvergence at the outflow boundaries of elements for nonlinear conservation laws and problems of the form (2.44) is currently under investigation. We plan to extend these results to locally refined meshes with hanging nodes and unstructured tetrahedral meshes for hyperbolic systems. Finally, we note that our error estimate does not apply near discontinuities.

Acknowledgements

Portions of this research were supported by the National Science Foundation (grant number DMS-0074174) and Sandia National Laboratories (contract number AW5657).

References

[1] S. Adjerid, K.D. Devine, J.E. Flaherty, L. Krivodonova, A posteriori error estimation for discontinuous Galerkin solutions of hyperbolic problems, Comput. Methods Appl. Mech. Engrg. 191 (2002) 1097–1112.

[2] F. Bassi, S. Rebay, A high-order accurate discontinuous finite element method for the numerical solution of the compressible Navier–Stokes equations, J. Computat. Phys. 131 (1997) 267–279.

[3] C.E. Baumann, J.T. Oden, A discontinuous hp finite element method for convection-diffusion problems, Comput. Methods Appl. Mech. Engrg. 175 (1999) 311–341.

[4] K.S. Bey, J.T. Oden, hp-version discontinuous Galerkin method for hyperbolic conservation laws, Comput. Methods Appl. Mech. Engrg. 133 (1996) 259–286.

[5] K.S. Bey, J.T. Oden, A. Patra, hp-version discontinuous Galerkin method for hyperbolic conservation laws: a parallel strategy, Int. J. Numer. Methods Engrg. 38 (1995) 3889–3908.

[6] K.S. Bey, J.T. Oden, A. Patra, A parallel hp-adaptive discontinuous Galerkin method for hyperbolic conservation laws, Appl. Numer. Math. 20 (1996) 321–386.

[7] R. Biswas, K. Devine, J.E. Flaherty, Parallel adaptive finite element methods for conservation laws, Appl. Numer. Math. 14 (1994) 255–284.

[8] B. Cockburn, A simple introduction to error estimation for nonlinear hyperbolic conservation laws, in: Proceedings of the 1998 EPSRC Summer School in Numerical Analysis, SSCM, Graduate Student's Guide for Numerical Analysis, vol. 26, Springer, Berlin, 1999, pp. 1–46.

[9] B. Cockburn, P.A. Gremaud, Error estimates for finite element methods for nonlinear conservation laws, SIAM J. Numer. Anal. 33 (1996) 522–554.

[10] B. Cockburn, G.E. Karniadakis, C.W. Shu (Eds.), Discontinuous Galerkin Methods Theory, Computation and Applications, Lectures Notes in Computational Science and Engineering, vol. 11, Springer, Berlin, 2000.

[11] B. Cockburn, S.Y. Lin, C.W. Shu, TVB Runge–Kutta local projection discontinuous Galerkin methods of scalar conservation laws III: One dimensional systems, J. Computat. Phys. 84 (1989) 90–113.

[12] B. Cockburn, C.W. Shu, TVB Runge–Kutta local projection discontinuous Galerkin methods for scalar conservation laws II: General framework, Math. Computat. 52 (1989) 411–435.

[13] K.D. Devine, J.E. Flaherty, Parallel adaptive hp-refinement techniques for conservation laws, Comput. Methods Appl. Mech. Engrg. 20 (1996) 367–386.

[14] K. Ericksson, C. Johnson, Adaptive finite element methods for parabolic problems I: A linear model problem, SIAM J. Numer. Anal. 28 (1991) 12–23.

[15] K. Ericksson, C. Johnson, Adaptive finite element methods for parabolic problems II: Optimal error estimates in $l_\infty l_2$ and $l_\infty l_\infty$, SIAM J. Numer. Anal. 32 (1995) 706–740.

[16] J.E. Flaherty, R. Loy, M.S. Shephard, B.K. Szymanski, J.D. Teresco, L.H. Ziantz, Adaptive local refinement with octree load-balancing for the parallel solution of three-dimensional conservation laws, J. Parallel Distrib. Comput. 47 (1997) 139–152.

[17] C. Johnson, Numerical Solution of Partial Differential Equations by the Finite Element Method, Cambridge University, New York, 1987.

[18] L. Krivodonova, J.E. Flaherty, Error estimation for discontinuous Galerkin solutions of multidimensional hyperbolic problems, submitted for publication. Proceedings of the Com^2 MaC Conference on Computational Mathematics, to appear.

[19] M. Larson, T. Barth, A posteriori error estimation for adaptive discontinuous Galerkin approximation of hyperbolic systems, in: B. Cockburn, G.E. Karniadakis, C.W. Shu (Eds.), Proceedings of the International Symposium on Discontinuous Galerkin Methods Theory, Computation and Applications, Springer, Berlin, 2000.

[20] W.H. Reed, T.R. Hill, Triangular mesh methods for the neutron transport equation, Technical Report LA-UR-73-479, Los Alamos Scientific Laboratory, Los Alamos, 1973.

[21] B. Rivière, M.F. Wheeler, A posteriori error estimation and mesh adaptation strategy for discontinuous Galerkin methods applied to diffusion problems, TICAM Report 00-10, 2000.

[22] E. Süli, A posteriori error analysis and adaptivity for finite element approximations of hyperbolic problems, in: D. Kröner, M. Ohlberger, C. Rhode (Eds.), An Introduction to Recent Developments in Theory and Numerics for Conservation Laws, Lecture Notes in Computational Sciences and Engineering, vol. 5, Springer, Berlin, 1999.

[23] M.F. Wheeler, An elliptic collocation-finite element method with interior penalties, SIAM J. Numer. Anal. 15 (1978) 152–161.